

PECCARY: A novel approach for characterizing orbital complexity, stochasticity, and regularity

SÓLEY Ó. HYMAN ¹, KATHRYNE J. DANIEL ¹ AND DAVID A. SCHAFFNER ²

¹*Steward Observatory and Department of Astronomy,
University of Arizona, 933 N. Cherry Ave., Tucson, AZ 85721, USA*

²*Bryn Mawr College
Department of Physics
Bryn Mawr, PA 19010, USA*

(Received July 17, 2024; Revised ??; Accepted ??)

ABSTRACT

KEYWORDS

PECCARY is a novel approach for characterizing orbital complexity, stochasticity, and regularity. It is designed to be used on a wide range of dynamical systems, including those with mixed phase space and chaotic regions. The method is based on the analysis of the system's phase space structure, identifying regions of regular motion and chaotic regions. The results are presented in a clear and concise manner, allowing for easy interpretation and comparison of different systems. The method is applied to a variety of systems, including the solar system, and the results are compared with other methods. The method is shown to be effective in identifying regions of regular motion and chaotic regions, and in characterizing the complexity and stochasticity of the system's motion.

Keywords: ~~2003~~ ~~0591~~ ~~6184~~ ~~61175~~ ~~61916~~ ~~6190~~

1. INTRODUCTION

The study of dynamical systems is a central topic in celestial mechanics and astrophysics. In particular, understanding the complex behavior of systems with mixed phase space is a major challenge. This paper introduces a new method, PECCARY, designed to address this challenge. The method is based on the analysis of the system's phase space structure, identifying regions of regular motion and chaotic regions. The results are presented in a clear and concise manner, allowing for easy interpretation and comparison of different systems. The method is applied to a variety of systems, including the solar system, and the results are compared with other methods. The method is shown to be effective in identifying regions of regular motion and chaotic regions, and in characterizing the complexity and stochasticity of the system's motion.

PECCARY is a novel approach for characterizing orbital complexity, stochasticity, and regularity. It is designed to be used on a wide range of dynamical systems, including those with mixed phase space and chaotic regions. The method is based on the analysis of the system's phase space structure, identifying regions of regular motion and chaotic regions. The results are presented in a clear and concise manner, allowing for easy interpretation and comparison of different systems. The method is applied to a variety of systems, including the solar system, and the results are compared with other methods. The method is shown to be effective in identifying regions of regular motion and chaotic regions, and in characterizing the complexity and stochasticity of the system's motion.

Corresponding author: Sóley Hyman, Kathryne J. Daniel
soleyhyman@arizona.edu, kjdaniel@arizona.edu

$N = 19$

$n = 5$

n

$$t_{pat} = \ell \delta t (n - 1), \quad (1)$$

δt

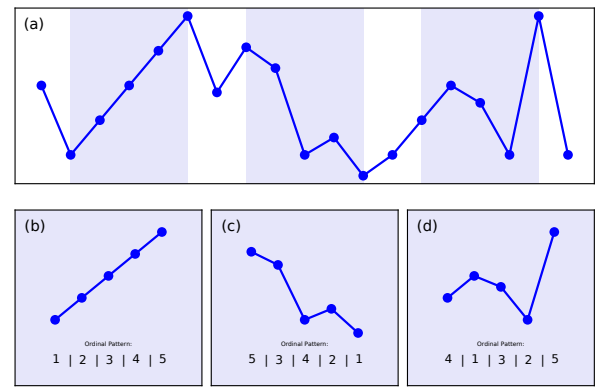


Figure 1. An arbitrary time-series of $N = 19$ discrete points used to construct embedding dimension $n = 5$ ordinal patterns. Shaded regions in panel (a) indicate three examples of patterns using sampling interval $\ell = 1$. Shaded points in panels (b)-(d) show the ordinal pattern from lowest value (bottom) to highest value (top) of the five points within each shaded region. This ordinal pattern can be represented by the numerical sequence listed at the bottom of each panel.

(2002)

$n > 2$, (2002),

$n! \ll N$

$n \leq 7$.

$n = 5$

(2004; 2007; 2015).

2.2. Pattern Probability and Pattern Probability Distributions

$\ell(n - 1)$

P

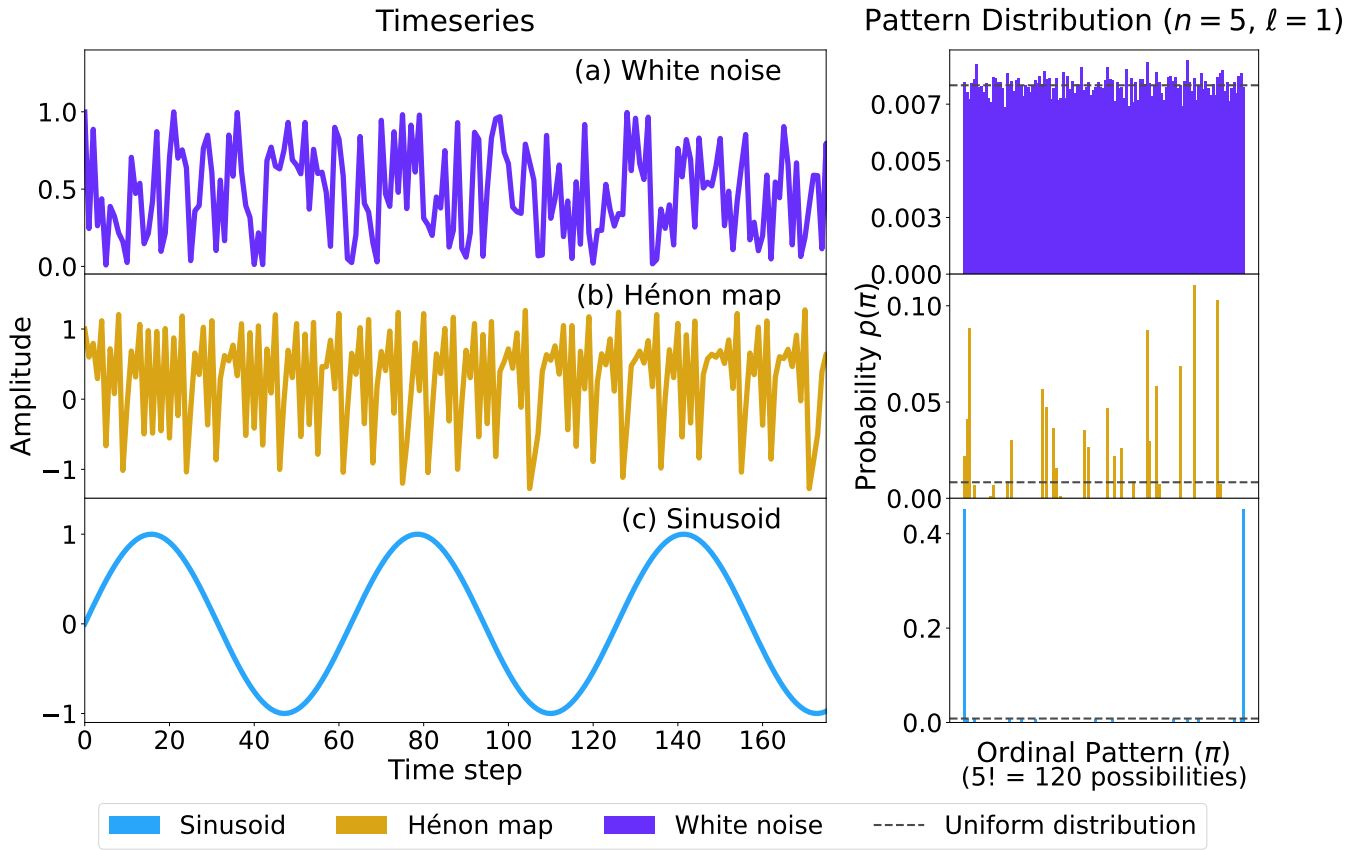


Figure 3. *Left:* Sample section of time-series from $t = 0$ to $t = 175$ out of $t = 0$ to $t = 5 \times 10^4$ for (a) white noise (stochastic), (b) Hénon Map (chaotic), and (c) sinusoidal (periodic), where the inset is a zoom-in of a short timescale segment of the series. *Right:* Ordinal pattern probability $p(\pi)$ for possible ordinal patterns π for each time-series given an sampling size $n = 5$ and sampling interval $\ell = 1$. The stochastic time-series has a uniform distribution of patterns, the periodic time-series has a small number of preferred patterns, and the chaotic time-series has a variety of preferred, underpreferred, and forbidden patterns.

$H_{\text{per}}^{\min}(n=5) = 0.14478.$
 $N_{\text{periodic}}(n) = 2\lfloor (n-2) + 1 \rfloor.$ (6)

$H_{\text{per}}^{\max}(n) = \frac{N_{\text{periodic}}(n)}{n!}.$ (7)

$N_{\text{periodic}}(n=5) = 14,$
 $H \leq H_{\text{per}}^{\max} = 0.55124.$

$< n < 8.$
 2.3.2. Disequilibrium and Complexity
 P

Let P_e be the probability of error, $p_e = 1/n!$. Then P and P_e are related by

$$d[P, P_e] = S \left[\frac{P + P_e}{2} \right] - \frac{1}{2} S[P] - \frac{1}{2} S[P_e], \quad (8)$$

where $S[P + P_e]$ is the entropy of $P + P_e$. The distance $d(P, P_e)$ is normalized by d/d_{\max} (Sch 2004),

$$D[P, P_e] = \frac{2d[P, P_e]}{2 \log(n!) - \log(n!) - \frac{n!+1}{n!} \log(n!+1)}, \quad (9)$$

where $D \rightarrow 1$ as $H \rightarrow 0$. (Sch 2004; Sch 2007),

$$C[P, P_e] = D[P, P_e] H[P]. \quad (10)$$

The quantity C is the relative entropy of H to D (Sch 1995) (Sch 2004; Sch 2007), (Sch 1988). It is defined by (Sch 2004), see (Sch 2.4 & 4). It is defined by (Sch 2004; Sch 2007; Sch 2012).

2.4. The HC-Plane

The relative entropy C is a function of P and P_e .

H (Sch 2007). The relative entropy C is a function of H and P_e . The relative entropy C is a function of H and P_e . The relative entropy C is a function of H and P_e .

The relative entropy C is a function of H and P_e . The relative entropy C is a function of H and P_e . The relative entropy C is a function of H and P_e .

The relative entropy C is a function of H and P_e . The relative entropy C is a function of H and P_e . The relative entropy C is a function of H and P_e .

$$(x_m, y_m) = \begin{cases} x_{m+1} = 1 - ax_m^2 + y_m \\ y_{m+1} = bx_m \end{cases}, \quad (11)$$

The relative entropy C is a function of H and P_e . The relative entropy C is a function of H and P_e . The relative entropy C is a function of H and P_e .

3. PECCARY

3.1. Setting up PECCARY

The relative entropy C is a function of H and P_e . The relative entropy C is a function of H and P_e . The relative entropy C is a function of H and P_e .

Table 1. Glossary of Statistical Terms

Symbol	Name	Definition	Eq. no
P	Pattern probability distribution	All possible $n!$ ordinal pattern permutations	§2.2
P_e	Equilibrium pattern probability distribution	Uniform distribution of all possible $n!$ ordinal pattern permutations	§2.3.2
π_i	i -th ordinal pattern	A possible pattern permutation of the pattern probability distribution P	§2.2
S	Shannon Entropy	Information entropy	§2.3.1, Eq. 3
H	Permutation Entropy	Normalized Shannon Entropy, measure used in HC -plane analysis	§2.3.1, Eq. 4
$H_{\text{per}}^{\min}(n)$	Minimum possible Permutation Entropy for a periodic function	Smallest value of H for a periodic function (e.g., sine wave); dependent on sampling size	§2.3.1, Eq. 5
$H_{\text{per}}^{\max}(n)$	Maximum possible Permutation Entropy for a periodic function	Largest value of H for a periodic function (e.g., sine wave); dependent on sampling size	§2.3.1, Eq. 7
$H(\ell)$	H-curve	Permutation Entropy as a function of the sampling interval	§3.2
d	Disequilibrium	Measure of how far pattern probability distribution P is from a uniform distribution of patterns	§2.3.2, Eq. 8
D	Normalized disequilibrium	Normalized measure of disequilibrium used in calculation of C	§2.3.2, Eq. 9
C	Jensen-Shannon Statistical Complexity	Measure used in HC -plane analysis	§2.3.2, Eq. 10
$C(\ell)$	C-curve	Statistical Complexity as a function of the sampling interval	§3.2

¹ <https://github.com/solehyman/chaos-orbits>

² <https://peccary.readthedocs.io>

is also discussed

with $n = 5$ (see 2.1).

is discussed

in the

paper

in the

paper

in the

3.2. Idealized Sampling Scheme and Limitations

is discussed

in the

paper

in the

paper

in the

paper

in the

² A

is discussed

in the

paper

in the

paper

in the

paper

in the

paper

in the

paper

in the

paper

in the

paper

in the

paper

in the

paper

in the

paper

in the

paper

ℓ , is also

t_{dur} , is also

t_{pat} is also

t_{nat} , is also

¹ <https://github.com/solehyman/chaos-orbits>

² <https://peccary.readthedocs.io>

$t_{\text{dur}}/t_{\text{nat}}$ is also

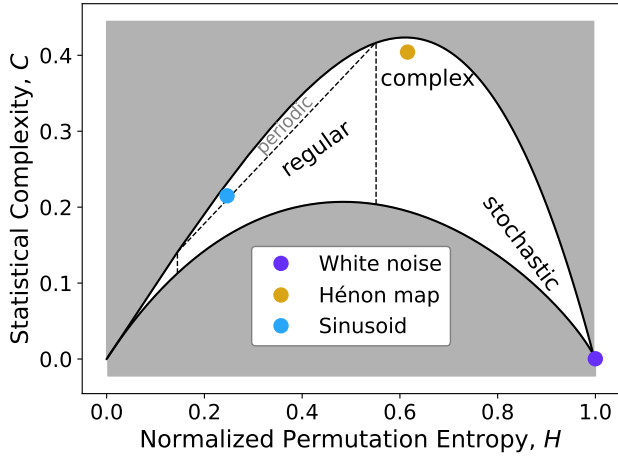


Figure 4. The HC -plane is an effective visualization of Permutation Entropy and Statistical Complexity, where the value for the Permutation Entropy H , for a time-series assuming given sampling interval is plotted on the x-axis and the value for Statistical Complexity C , is plotted on the y-axis. The upper and lower limits for C are indicated by the solid (black) crescent shaped curves, here specifically for $n = 5$. The relative scale of these boundaries depends on the embedding dimension, though it varies only slightly $n = 3$ through $n = 6$. The regions are associated with stochasticity fall in the lower right, while those associated with complex behavior fall in the upper central part of the plane. The dashed line indicates the boundary for the region for a purely periodic function, with the regular orbits outside of it. The $[H, C]$ coordinates are shown for the time-series in Figure 3 with sampling size $n = 5$ and sampling interval $\ell = 1$. Vertical dashed lines represent the minimum and maximum Permutation Entropy values for a purely periodic function (i.e., H_{per}^{\min} and H_{per}^{\max}).

3.2.1. Minimum time-series duration, $t_{\text{dur}}/t_{\text{nat}}$

$t_{\text{dur}}/t_{\text{nat}} = 0.5 - 10$.

$t_{\text{pat}}/t_{\text{nat}} = 0.1 - 0.7$.

H_{per}^{\min}

3.2.2. Timescale resolution, $t_{\text{pat}}/t_{\text{nat}}$

$t_{\text{pat}}/t_{\text{nat}} = 0.1 - 0.7$.

H_{per}^{\max}

$t_{\text{dur}}/t_{\text{nat}} \sim 1.5$.

3.2.3. Recommended sampling scheme constraints

$t_{\text{pat}}/t_{\text{nat}} \sim 0.25$.

$t_{\text{dur}}/t_{\text{nat}} = 1.5$.

[H, C] (ie, $t_{dur}/t_{nat} \gtrsim 1.5$, $0.3 \lesssim t_{pat}/t_{nat} \lesssim 0.5$. In $n = 5$ $n. \beta$ ℓ .

$H(\ell=1)$ $H-$ $H(\ell) \rightarrow$ H_{per}^{max} $t_{pat}/t_{nat} \sim 0.6$ C C $H)$, $HC-$

3.3. Interpreting PECCARY Values

$H(\ell)$ $C(\ell)$ $H-$ $C-$ $H(\ell)$ $C(\ell)$ t_{dur} $H(\ell) \sim 1$ $C(\ell) \sim 0$.

$\ell = 1$. $\ell = 1$. $H-$ $C-$ $H(\ell)$ $C(\ell)$ t_{pat}/t_{nat} $\delta t = 2^{-8}$ $t_{dur} = 10$ $t_{dur}/t_{nat} > 5$.

$H-$ $C-$ t_{pat}/t_{nat} $HC-$ $H-$ $C-$ t_{pat}/t_{nat} $H(\ell)$ $C(\ell)$ t_{dur} $H(\ell) \sim 1$ $C(\ell) \sim 0$.

4. Well-Characterized Mathematical Examples

4.1.1. Sine wave $\delta t = 2^{-8}$ $t_{dur} = 10$ $t_{dur}/t_{nat} > 5$.

$H(\ell)$ $C(\ell)$ t_{pat}/t_{nat} $\delta t = 2^{-8}$ $t_{dur} = 10$ $t_{dur}/t_{nat} > 5$.

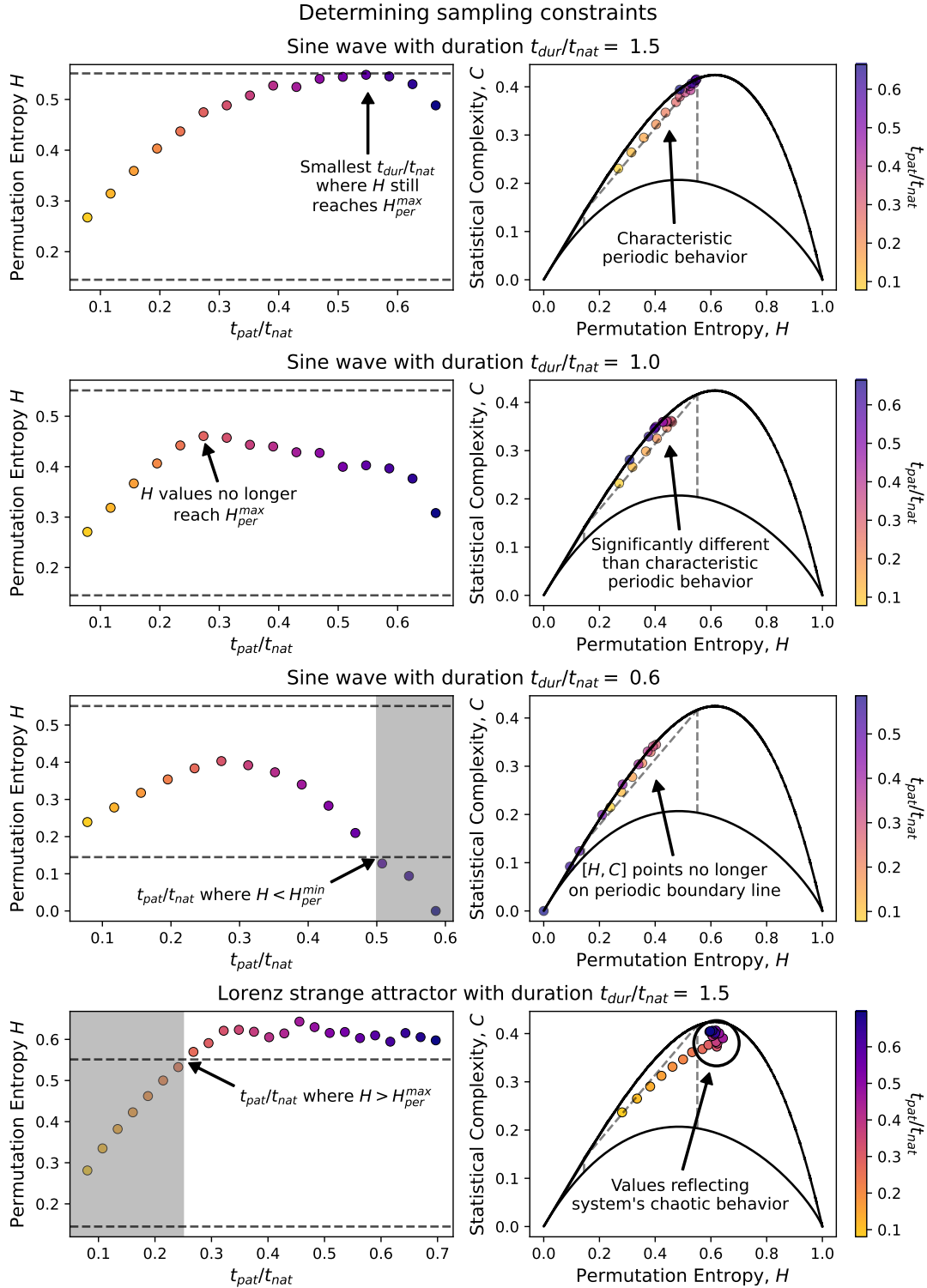


Figure 5. Illustration of method diagnostic for identifying sampling scheme constraints. *Top row:* $H(t_{pat}/t_{nat})$ and HC -plane plots for a sine wave time-series with a duration of $t_{dur}/t_{nat} = 1.5$, with t_{nat} being the period of the sinusoid. The HC -plane on the right demonstrates the characteristic behavior of a periodic function, and the H -curve plot on the left shows that $H(t_{pat}/t_{nat})$, or $H(\ell)$ does not reach the H_{per}^{max} upper limit. *Second row:* $H(t_{pat}/t_{nat})$ and HC -plane plots for a sine wave time-series with $t_{dur}/t_{nat} = 1$, i.e., $t_{dur} = t_{nat}$. Both H -curve and HC -plane plots show that behavior deviates significantly from the characteristic behavior. *Third row:* $H(t_{pat}/t_{nat})$ and HC -plane plots for a sine wave time-series with $t_{dur}/t_{nat} = 0.6$. H -curve shows the value for t_{pat}/t_{nat} at which $H < H_{per}^{min}$. Points on HC -plane do not fall on the periodic boundary line. *Fourth row:* $H(t_{pat}/t_{nat})$ and HC -plane plots for a chaotic Lorenz strange attractor time-series with $t_{dur}/t_{nat} = 1.5$. H -curve shows the location at which $H(t_{pat}/t_{nat}) > H_{per}^{max}$, indicating the region where the chaotic time-series is reliably classified as complex. A circle on the HC -plane marks the accurately-classified points.

Table 2. Glossary of Sampling Terms and Timescales

Parameter Type	Symbol	Name	Definition	Eq. no
Sampling	n	Sampling size	Number of data points for each extracted pattern (i.e., sampling window)	§2.1
	ℓ	Sampling interval	Number of points in between each extracted point (i.e., sampling interval)	§2.1
Timescales	δt	Time-step	Time element associated with a single step in the time-series	§2.1
	t_{pat}	Pattern Timescale	Timescale for an ordinal pattern	§2.1, Eq. 1
	t_{dur}	Time-series duration	Total duration for a time-series	§3.2
	t_{nat}	Natural timescale	Natural or approximate period of oscillation for the system	§3.2

$H^{\max}_{\text{periodic}}$
 $HC-\mathfrak{p}(\mathfrak{p})$
 l

4.1.2. *Noise varieties*

ν , h
 $\propto \nu$, $h(\nu$
 $\propto \nu^2)$, $h(\nu$
 $\propto \nu^{-2})$, $h(\nu$
 $\propto \nu^{-1})$.
 examples.noiseColors
 10^4

$HC-\mathfrak{p}$
 $H(\ell)$ d $C(\ell)$
 C isom
 H isom
 $HC-\mathfrak{p}$
 l , h

4.1.3. *Chaotic systems*

$\mathfrak{p}(E11)$
 $\mathfrak{p}(1963)$,
 $\frac{dx}{dt} = \sigma(y - x)$ (12)
 $\frac{dy}{dt} = x(\rho - z) - y$ (13)
 $\frac{dz}{dt} = xy - \beta z$ (14)

$\sigma = 10$, $\rho = 20$, $\beta = \frac{8}{3}$,
 1963
 n, a

3.2
 t_{nat}
 t_{pat}
 $t_{\text{pat}}/t_{\text{nat}}$
 t_{nat}
 t_{pat}
 $C(\ell)$
 t_{pat}
 t_{nat}
 $C(\ell)$
 $H(\ell)$ d $C(\ell)$
 H step
 $HC-\mathfrak{p}$

4.2. *Double Pendulum*

examples.doublePendulum
 1
 2.5 5

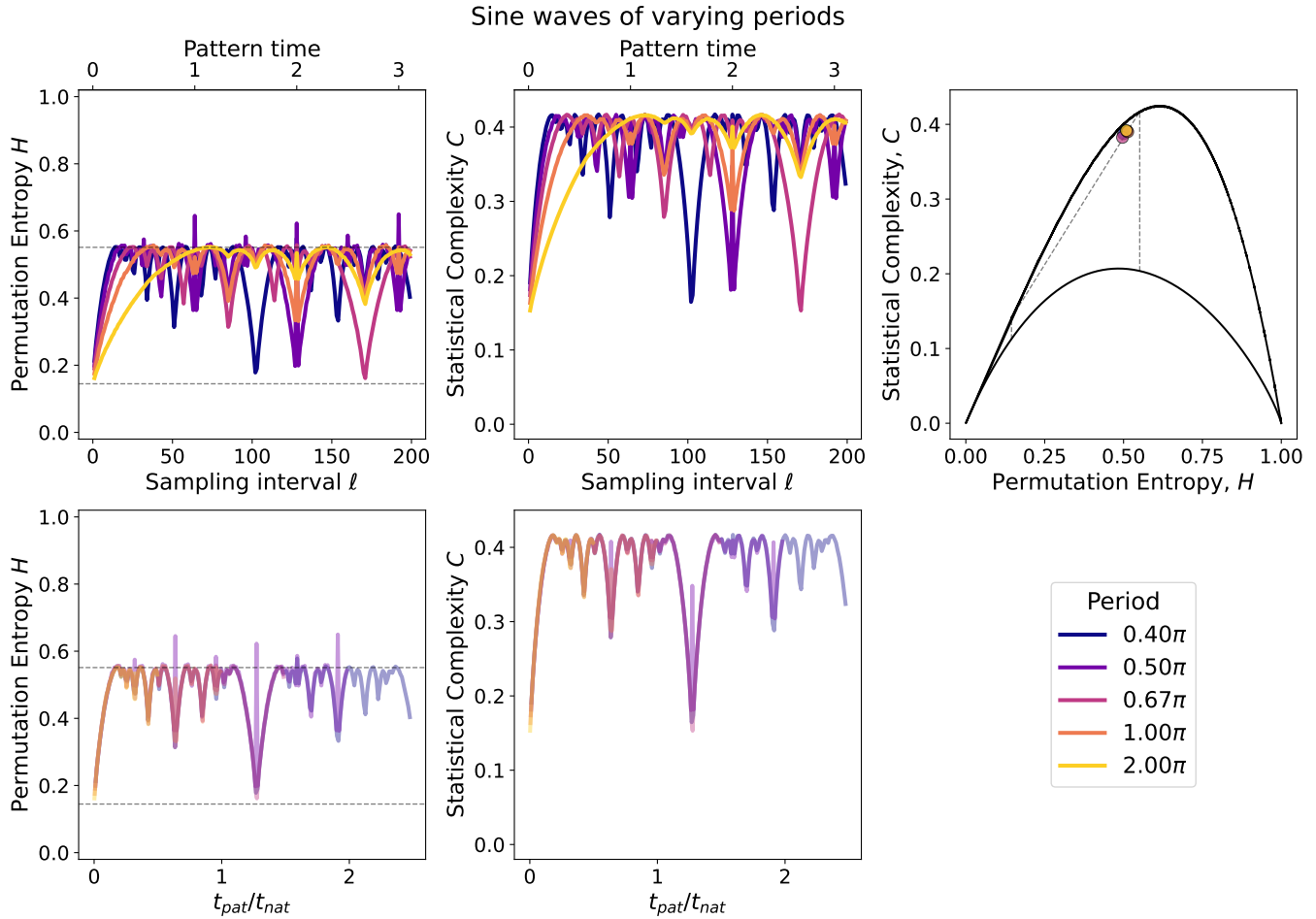


Figure 6. Permutation Entropy and Statistical Complexity values for a range of sampling intervals for five sine waves of different periods. *Top left panel:* Permutation Entropy values for sampling intervals ranging from 1 to 200, with the corresponding pattern timescales on the top x-axis. Sine waves with smaller periods reach the $H_{\text{per}}^{\text{max}}(n=5)$ limit more quickly. Horizontal dashed lines in the two left panels represent the upper and lower limits of $H_{\text{per}}^{\text{min}}(n=5)$ and $H_{\text{per}}^{\text{max}}(n=5)$, respectively. *Bottom left panel:* The same Permutation Entropy values except that the x-axis is the pattern timescale scaled by the period of each sine wave (i.e., $t_{\text{pat}}/t_{\text{nat}}$). All five of the H-curves overlap exactly, with the exception of the numerical spikes. *Top center panel:* Statistical Complexity values as a function of sampling interval/pattern timescale. As with the H-curves, the sine waves with shorter periods reach the initial peak much more rapidly than those with longer periods. *Bottom center panel:* Statistical Complexity values plotted against the $t_{\text{pat}}/t_{\text{nat}}$ ratio show that the C-curves for the different sine waves have the same functional form. *Top right panel:* The H and C values for the five sine waves with ideal sampling ($t_{\text{pat}}/t_{\text{nat}} = 0.4$, $t_{\text{dur}}/t_{\text{nat}} \geq 1$) plotted on the HC -plane all fall on or within the boundary region for a pure periodic function.

10 $\delta t = 2^{-6}$ s
 (eg 5 s) $\delta t = 2^{-6}$ s
 (eg 2.5 s) $\delta t = 2^{-6}$ s
 (eg 50 s) $\delta t = 2^{-6}$ s
 (eg 100 s) $\delta t = 2^{-6}$ s
 (eg 200 s) $\delta t = 2^{-6}$ s
 (eg 500 s) $\delta t = 2^{-6}$ s
 (eg 1000 s) $\delta t = 2^{-6}$ s
 (eg 2000 s) $\delta t = 2^{-6}$ s
 (eg 5000 s) $\delta t = 2^{-6}$ s
 (eg 10000 s) $\delta t = 2^{-6}$ s

HC-plot
 H, C plot

4.3. Astrophysical Examples

galpy (B2015), symplec4.c

4.3.1. Keplerian Potential

Keplerian Potential
 (ie, K_p)
 galpy (B2015),
 symplec4.c

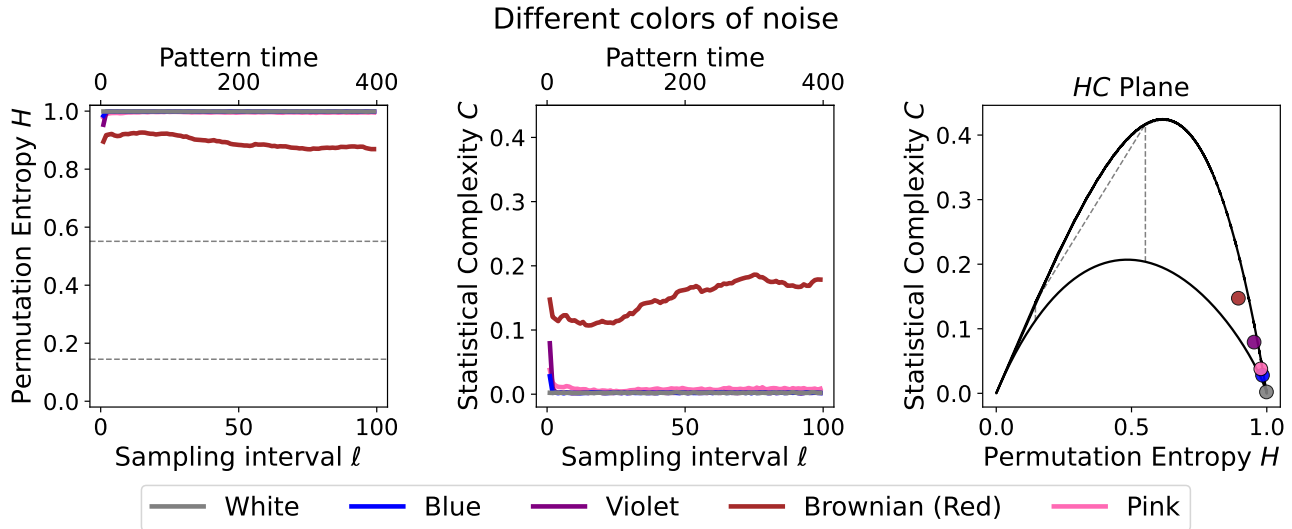


Figure 7. Permutation Entropy and Statistical Complexity values for a range of sampling intervals for five different colors of noise (pink, red, violet, blue, and white). *Left panel:* Permutation Entropy as a function of sampling interval/pattern timescale. All H values are very high (close to $H = 1$), indicating the presence of close to all possible permutations of patterns. Horizontal dashed lines represent the upper and lower limits of $H_{\text{per}}^{\min}(n = 5)$ and $H_{\text{per}}^{\max}(n = 5)$, respectively. *Center panel:* Statistical Complexity as a function of sampling interval/pattern timescale. C values are very low for all colors of noise, indicating that the pattern probability distributions are close to uniform. *Right panel:* The $[H, C]$ values for sampling interval of $\ell = 1$ plotted on the HC -plane for all noise varieties fall well within the stochastic region.

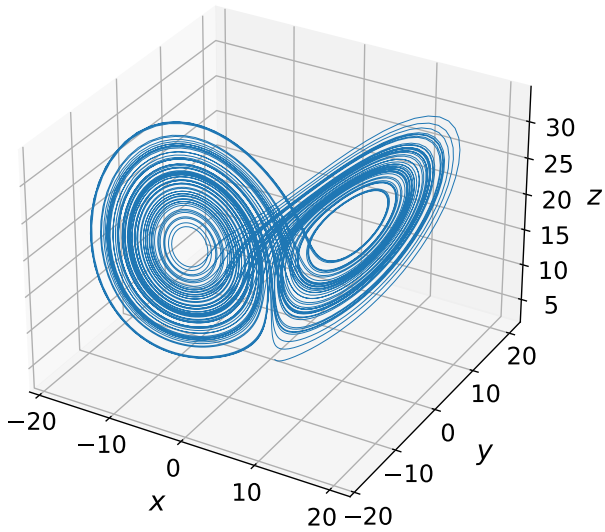


Figure 8. Three dimensional plot of the Lorenz strange attractor with parameters $\sigma = 10$, $\rho = 20$, and $\beta = 2.667$.

```

100 galpy's
orbit = galpy.Orbit.from_name('solar system')
orbit.plot()

```

HC -high

4.3.2. Globular Cluster

```

A globular cluster is a
dense collection of stars
in a spherical shape.
(galpy.potential.PlummerPotential)
from galpy.potential import PlummerPotential
p = PlummerPotential(
    galpy.df.isotropicPlummerdf), 10^4
p.plot()

```

HC -mid

H, C

```

tdur/tpat >= 1.5 and tpat/tnat = 0.4

```

```

galpy's
orbit = galpy.Orbit.from_name('solar system')
orbit.plot()

```

4.3.3. Triaxial Halo

```

A triaxial halo is a
dense collection of stars
in a triaxial shape.

```

```

galpy's
Orbit.from_name('solar system')
orbit.plot()

```

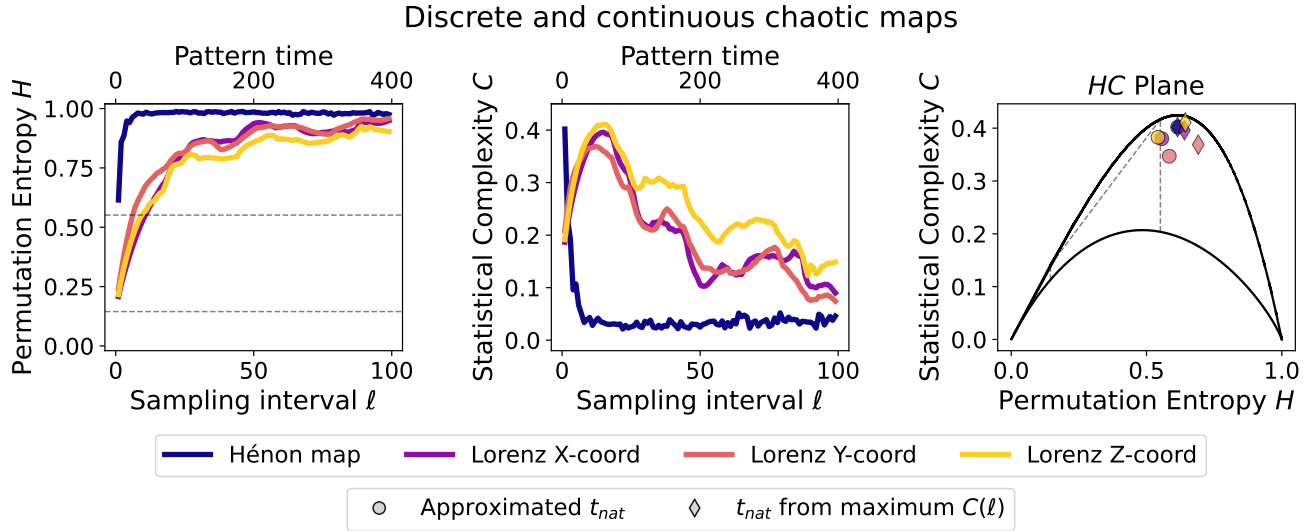


Figure 9. Permutation Entropy and Statistical Complexity values for a range of sampling intervals for the discrete Hénon map and the continuous x/y/z-coordinates of the Lorenz strange attractor. *Left panel:* Permutation Entropy as a function of sampling interval/pattern timescale. For all time-series, the H values increase initially and approach 1 rapidly (for a discrete chaotic system) or gradually (for a continuous chaotic system). Horizontal dashed lines represent the upper and lower limits of $H_{per}^{min}(n=5)$ and $H_{per}^{max}(n=5)$, respectively. *Center panel:* Statistical Complexity as a function of sampling interval/pattern timescale. For the discrete chaotic map, the C values drop rapidly and bottom out close to zero. With the continuous chaotic map, the values of C initially increase and then gradually decrease. *Right panel:* The $[H, C]$ values plotted on the HC -plane for the different chaotic systems span across the HC -plane at ideal sampling. $[H, C]$ points calculated using the “approximated t_{nat} ” method are shown as circles, while those determined with the “ t_{nat} from maximum $C(l)$ ” method are represented as diamonds. All values fall within the chaotic regime.

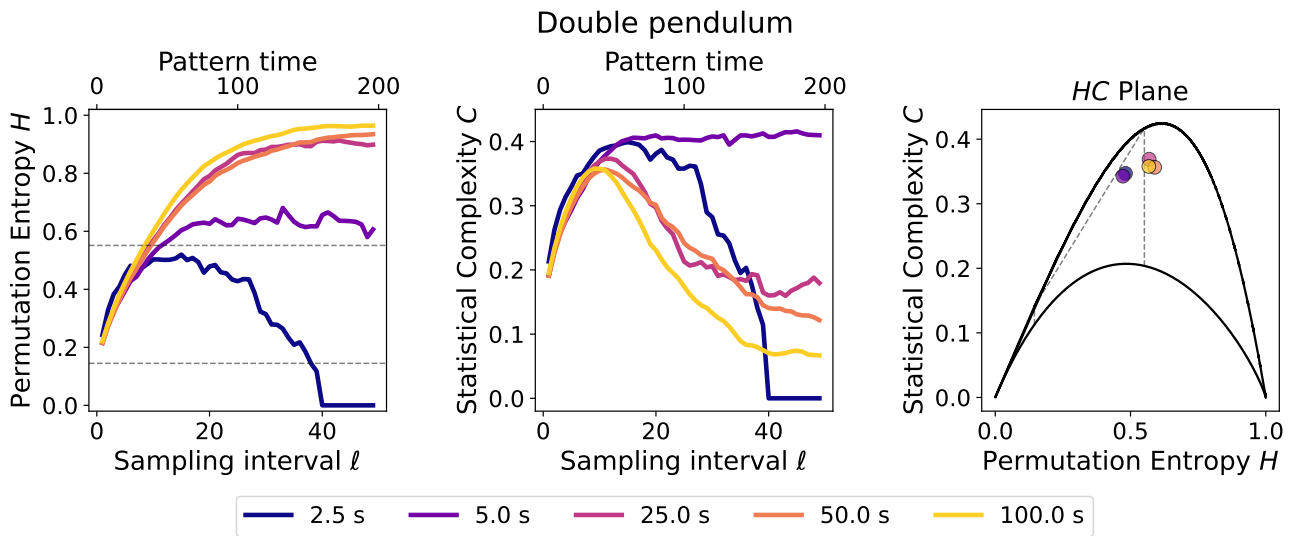


Figure 10. Permutation Entropy and Statistical Complexity values for a range of sampling intervals for the double pendulum. *Left panel:* Permutation Entropy as a function of sampling interval/pattern timescale. For all time-series, the H values increase gradually. Horizontal dashed lines represent the upper and lower limits of $H_{per}^{min}(n=5)$ and $H_{per}^{max}(n=5)$, respectively. *Center panel:* Statistical Complexity as a function of sampling interval/pattern timescale. For all simulation durations, the values of C initially increase and then gradually decrease, with the exception of the shortest simulations. *Right panel:* The $[H, C]$ values plotted on the HC -plane for the different simulation durations at ideal sampling. All values fall within the complex regime, with the exception of the 2.5 s simulation.

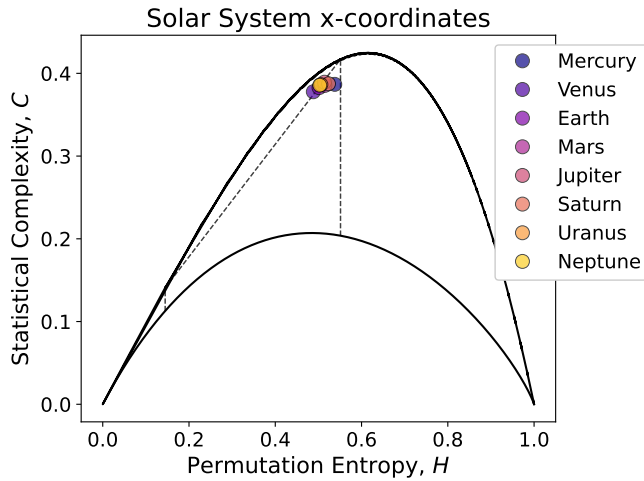


Figure 11. HC -plane showing the $[H, C]$ coordinates for tracer particle simulation x-coordinates of the Solar System when $t_{\text{pat}}/t_{\text{nat}} = 0.4$. All data points fall within the periodic/regular boundary, consistent with the fact that these are circular orbits.

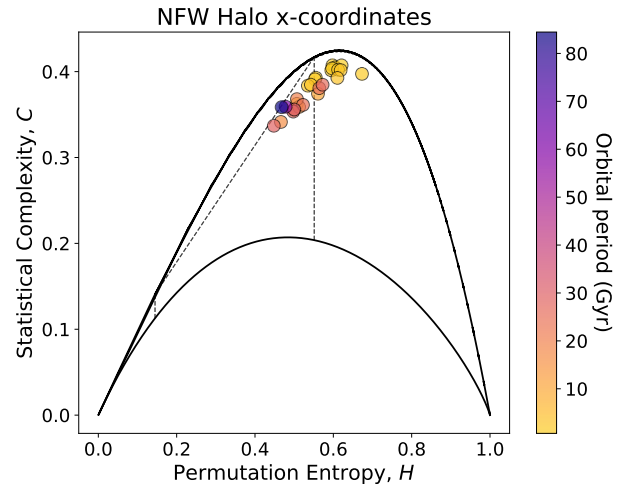


Figure 13. HC -plane showing the $[H, C]$ values when $t_{\text{pat}}/t_{\text{nat}} = 0.4$ for triaxial NFW halo tracer particles. The x-coordinates are used for the PECCARY method, with orbital periods satisfying the $t_{\text{dur}}/t_{\text{nat}} \geq 1.5$ requirement. As expected for a triaxial potential, there is a mix particles falling in both the regular and complex zones.

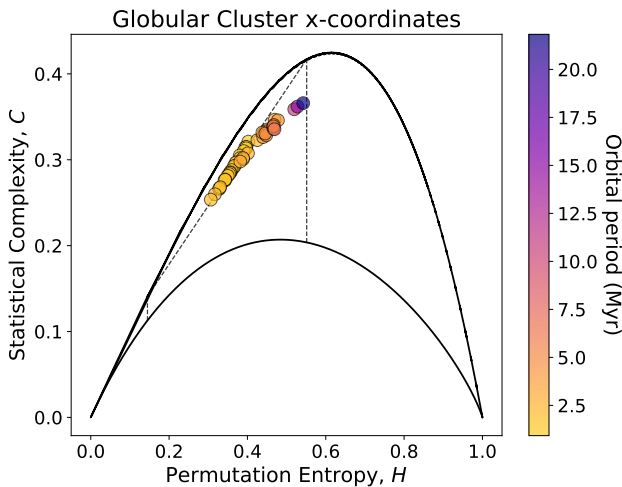


Figure 12. HC -plane showing the $[H, C]$ values when $t_{\text{pat}}/t_{\text{nat}} = 0.4$ for globular cluster tracer particles. The x-coordinates are used for the PECCARY method, with orbital periods satisfying the $t_{\text{dur}}/t_{\text{nat}} \geq 1.5$ requirement. Most of the $[H, C]$ values fall on or within the periodic/regular boundary/region, though some have lower complexity values. None of the $[H, C]$ values for the orbits exceed the $H_{\text{per}}^{\text{max}}$ limit for $n = 5$, consistent with the expectation that all of the orbits for a spherical potential are regular.

```

import numpy as np
from galpy.potential.TriaxialNFWPotential import TriaxialNFWPotential
from galpy.potential.IsotropicNFWPotential import IsotropicNFWPotential
from galpy.df import DF, DFAction

# Create a triaxial NFW potential
triauxial = TriaxialNFWPotential(
    a=10, b=1.66, c=3.16,
    M=15.625,
    G=1)

# Create an isotropic NFW potential
isotropic = IsotropicNFWPotential(
    a=10, M=15.625, G=1)

# Create a DF for the triaxial potential
df = DF(
    N=10000,
    mass=1,
    potential=triaxial,
    G=1)
    
```

```

import numpy as np
import matplotlib.pyplot as plt
from galpy.potential.TriaxialNFWPotential import TriaxialNFWPotential
from galpy.potential.IsotropicNFWPotential import IsotropicNFWPotential
from galpy.df import DF, DFAction

# Create a triaxial NFW potential
triaxial = TriaxialNFWPotential(
    a=10, b=1.66, c=3.16,
    M=15.625,
    G=1)

# Create an isotropic NFW potential
isotropic = IsotropicNFWPotential(
    a=10, M=15.625, G=1)

# Create a DF for the triaxial potential
df = DF(
    N=10000,
    mass=1,
    potential=triaxial,
    G=1)

# Simulate the DF
df.integrate(
    t_start=0, t_end=10,
    dt=0.1)

# Plot the HC-plane
H, C = df.getHAndC()
plt.scatter(H, C, c=df.getOrbitalPeriod(), s=10)

# Add the periodic/regular boundary
H_per_max = 0.55
C_per_max = 0.21
plt.plot([0, H_per_max, 1], [0, C_per_max, 0])
plt.plot([0, H_per_max, 1], [0, 0.21, 0])
    
```

4.3.4. Injected Noise

```

import numpy as np
import matplotlib.pyplot as plt
from galpy.potential.TriaxialNFWPotential import TriaxialNFWPotential
from galpy.potential.IsotropicNFWPotential import IsotropicNFWPotential
from galpy.df import DF, DFAction

# Create a triaxial NFW potential
triaxial = TriaxialNFWPotential(
    a=10, b=1.66, c=3.16,
    M=15.625,
    G=1)

# Create an isotropic NFW potential
isotropic = IsotropicNFWPotential(
    a=10, M=15.625, G=1)

# Create a DF for the triaxial potential
df = DF(
    N=10000,
    mass=1,
    potential=triaxial,
    G=1)

# Simulate the DF
df.integrate(
    t_start=0, t_end=10,
    dt=0.1)

# Add injected noise
df.addNoise(
    noise=0.1,
    t_start=5, t_end=10)

# Plot the HC-plane
H, C = df.getHAndC()
plt.scatter(H, C, c=df.getOrbitalPeriod(), s=10)

# Add the periodic/regular boundary
H_per_max = 0.55
C_per_max = 0.21
plt.plot([0, H_per_max, 1], [0, C_per_max, 0])
plt.plot([0, H_per_max, 1], [0, 0.21, 0])
    
```


$t_{pat}/t_{nat} = 0.4$
 H, C
 100%
 50%
 100%

HC
 $t_{dur}/t_{nat} \geq 1.5$
 $H, C]$
 $H, C]$

H
 C
 HC

5. ℓ

$\ell = 1$

$H(\ell)$
 $C(\ell)$
 $t_{dur}/t_{nat} \gtrsim 1.5$
 $H(\ell)$

$.3 \lesssim t_{pat}/t_{nat} \lesssim 0.5$

(6.4.3),
 (1990; IV
 (1998; 2012, 2016; 2019, 2023)

3

4
 5

3.4

- 1
- 2
- 3
- 4
- 5
- 6
- 7
- 8
- 9

³ <https://peccary.readthedocs.io>
⁴ <https://github.com/solehyman/peccary>
⁵ <https://pypi.org/project/peccary/>

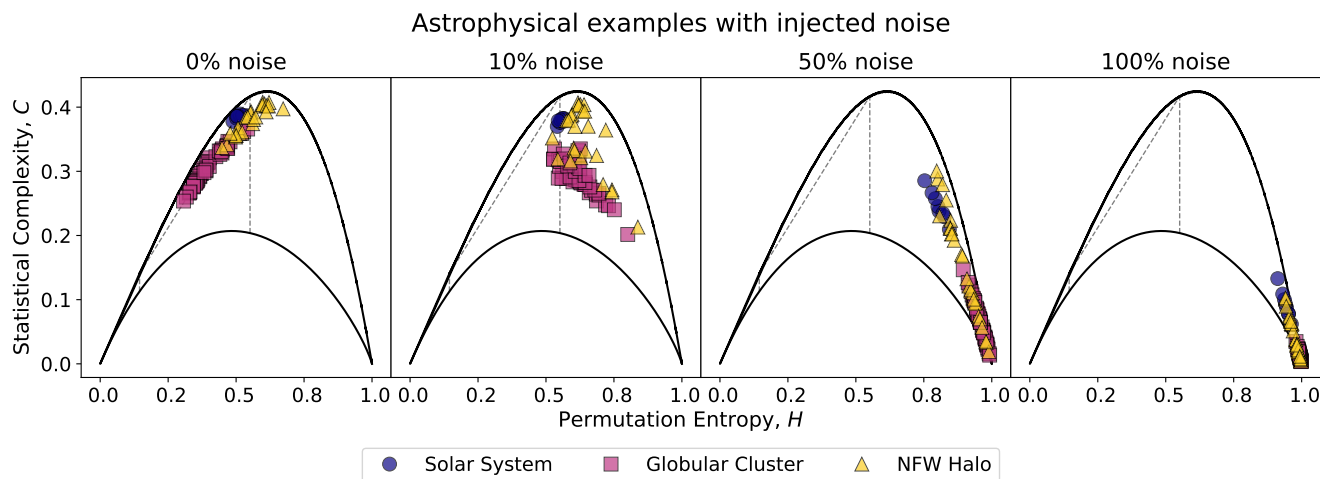


Figure 14. HC -planes showing the effect of noise injection on the PECCARY method for the three astrophysical example potentials. Circle, square, and triangle markers represent the Solar System, globular cluster, and triaxial halo simulations respectively. *Left panel:* Original $[H, C]$ values, as shown in Figures 11-13. *Left-center panel:* $[H, C]$ values for the three potentials with noise amplitude at 10% of the signal amplitude. Regular orbits appear to fall either within the regular region or below the primary complex region. Complex orbits still fall within the region of maximum complexity. *Right-center panel:* $[H, C]$ values for the three potentials with noise amplitude at 50% of the signal amplitude. Almost all of the values appear to fall within the stochastic region. *Right panel:* $[H, C]$ values for the three potentials with noise amplitude equal to the signal amplitude. All of the values to fall within the stochastic region.

Software: [10.21203/rs.3.rs-36581/v1](https://doi.org/10.21203/rs.3.rs-36581/v1)

E

- Araujo, F. H. A. d., Bejan, L., Stosic, B., & Stosic, T. 2020, *Chaos, Solitons Fractals*, 139, 110081, doi: <https://doi.org/10.1016/j.chaos.2020.110081>
- Aronis, K. N., Berger, R. D., Calkins, H., et al. 2018, *Chaos*, 28, 063130, doi: [10.1063/1.5023588](https://doi.org/10.1063/1.5023588)
- Astakhov, S. A., Burbanks, A. D., Wiggins, S., & Farrelly, D. 2003, *Nature*, 423, 264, doi: [10.1038/nature01622](https://doi.org/10.1038/nature01622)
- Athanassoula, E., Bienayme, O., Martinet, L., & Pfenniger, D. 1983, *A&A*, 127, 349
- Bandt, C., & Pompe, B. 2002, *Phys. Rev. Lett.*, 88, 174102, doi: [10.1103/PhysRevLett.88.174102](https://doi.org/10.1103/PhysRevLett.88.174102)
- Bariviera, A. F., Zunino, L., Guercio, M. B., Martinez, L. B., & Rosso, O. A. 2013, *J. Stat. Mech. Theory Exp.*, 2013, P08007, <http://stacks.iop.org/1742-5468/2013/i=08/a=P08007>
- Beraldo e Silva, L., de Siqueira Pedra, W., Valluri, M., Sodr e, L., & Bru, J.-B. 2019, *ApJ*, 870, 128, doi: [10.3847/1538-4357/aaf397](https://doi.org/10.3847/1538-4357/aaf397)
- Beraldo e Silva, L., Debattista, V. P., Anderson, S. R., et al. 2023, *ApJ*, 955, 38, doi: [10.3847/1538-4357/ace976](https://doi.org/10.3847/1538-4357/ace976)
- Bovy, J. 2015, *ApJS*, 216, 29, doi: [10.1088/0067-0049/216/2/29](https://doi.org/10.1088/0067-0049/216/2/29)
- Calbet, & Lopez-Ruiz, R. 2001, *Physical review. E, Statistical, nonlinear, and soft matter physics*, 63, 066116
- Cao, Y., Tung, W.-w., Gao, J. B., Protopopescu, V. A., & Hively, L. M. 2004, *PhRvE*, 70, 046217, <https://link.aps.org/doi/10.1103/PhysRevE.70.046217>
- Contopoulos, G. 1990, *Proceedings of the Royal Society of London Series A*, 431, 183, doi: [10.1098/rspa.1990.0126](https://doi.org/10.1098/rspa.1990.0126)
- Deck, K. M., Payne, M., & Holman, M. J. 2013, *ApJ*, 774, 129, doi: [10.1088/0004-637X/774/2/129](https://doi.org/10.1088/0004-637X/774/2/129)
- Dehnen, W. 2001, *MNRAS*, 324, 273, doi: [10.1046/j.1365-8711.2001.04237.x](https://doi.org/10.1046/j.1365-8711.2001.04237.x)
- Donner, R. V., Potirakis, S. M., Balasis, G., Eftaxias, K., & Kurths, J. 2015, *Physics and Chemistry of the Earth, Parts A/B/C*, 85-86, 44. <http://www.sciencedirect.com/science/article/pii/S1474706515000327>
- Fernandes, L. H., de Araujo, F. H., & Silva, M. A. 2020, *Research Square*, doi: [10.21203/rs.3.rs-36581/v1](https://doi.org/10.21203/rs.3.rs-36581/v1)
- Fux, R. 2001, *A&A*, 373, 511, doi: [10.1051/0004-6361:20010561](https://doi.org/10.1051/0004-6361:20010561)
- Gekelman, W., Compennolle, B. V., DeHaas, T., & Vincena, S. 2014, *Plasma Physics and Controlled Fusion*, 56, 064002, <http://stacks.iop.org/0741-3335/56/i=6/a=064002>
- Gekelman, W., Van Compennolle, B., DeHaas, T., & Vincena, S. 2014, *Plasma Physics and Controlled Fusion*, 56, 064002

- Gladman, B. 1993, *Icarus*, 106, 247, doi: [10.1006/icar.1993.1169](https://doi.org/10.1006/icar.1993.1169)
- Good, S. W., Ala-Lahti, M., Palmerio, E., Kilpua, E. K. J., & Osmane, A. 2020, *ApJ*, 893, 110, doi: [10.3847/1538-4357/ab7fa2](https://doi.org/10.3847/1538-4357/ab7fa2)
- Hénon, M. 1976, *Communications in Mathematical Physics*, 50, 69, doi: [10.1007/BF01608556](https://doi.org/10.1007/BF01608556)
- Hesp, C., & Helmi, A. 2018, arXiv e-prints, arXiv:1804.03670, doi: [10.48550/arXiv.1804.03670](https://doi.org/10.48550/arXiv.1804.03670)
- Jordan, D., Stockmanns, G., Kochs, E. F., Pilge, S., & Schneider, G. 2008, *Anesthesiology*, 109, 1014, doi: [10.1097/ALN.0b013e31818d6c55](https://doi.org/10.1097/ALN.0b013e31818d6c55)
- Kandrup, H. E., & Willmes, D. E. 1994, *A&A*, 283, 59
- Lamberti, P. W., Martin, M. T., Plastino, A., & Rosso, O. A. 2004, *Physica A: Statistical Mechanics and its Applications*, 334, 119
- Laskar, J. 1990, *Icarus*, 88, 266, doi: [10.1016/0019-1035\(90\)90084-M](https://doi.org/10.1016/0019-1035(90)90084-M)
- Laskar, J., Froeschlé, C., & Celletti, A. 1992, *Physica D Nonlinear Phenomena*, 56, 253, doi: [10.1016/0167-2789\(92\)90028-L](https://doi.org/10.1016/0167-2789(92)90028-L)
- Li, D., Li, X., Liang, Z., Voss, L. J., & Sleigh, J. W. 2010, *Journal of Neural Engineering*, 7, 046010, <http://stacks.iop.org/1741-2552/7/i=4/a=046010>
- Lithwick, Y., & Wu, Y. 2011, *ApJ*, 739, 31, doi: [10.1088/0004-637X/739/1/31](https://doi.org/10.1088/0004-637X/739/1/31)
- López-Ruiz, R., Mancini, H. L., & Calbet, X. 1995, *Physics Letters A*, 209, 321
- Lorenz, E. N. 1963, *Journal of the Atmospheric Sciences*, 20, 130, doi: [10.1175/1520-0469\(1963\)020<0130:DNF>2.0.CO;2](https://doi.org/10.1175/1520-0469(1963)020<0130:DNF>2.0.CO;2)
- Maggs, J. E., & Morales, G. J. 2013, *Plasma Physics and Controlled Fusion*, 55, 085015, <http://stacks.iop.org/0741-3335/55/i=8/a=085015>
- Maggs, J. E., Rhodes, T. L., & Morales, G. J. 2015, *Plasma Physics and Controlled Fusion*, 57, 045004, <http://stacks.iop.org/0741-3335/57/i=4/a=045004>
- Malhotra, R. 1993, *Nature*, 365, 819, doi: [10.1038/365819a0](https://doi.org/10.1038/365819a0)
- Manos, T., & Athanassoula, E. 2011, *MNRAS*, 415, 629, doi: [10.1111/j.1365-2966.2011.18734.x](https://doi.org/10.1111/j.1365-2966.2011.18734.x)
- Martinet, L. 1974, *A&A*, 32, 329
- Merritt, D., & Poon, M. Y. 2004, *ApJ*, 606, 788, doi: [10.1086/382497](https://doi.org/10.1086/382497)
- Murray-Clay, R. A., & Chiang, E. I. 2006, *ApJ*, 651, 1194, doi: [10.1086/507514](https://doi.org/10.1086/507514)
- Neyrinck, M., Genel, S., & Stücker, J. 2022, arXiv e-prints, arXiv:2206.10666, doi: [10.48550/arXiv.2206.10666](https://doi.org/10.48550/arXiv.2206.10666)
- Olivier, C. P., Engelbrecht, N. E., & Strauss, R. D. 2019, *Journal of Geophysical Research: Space Physics*, 124, 4, doi: [10.1029/2018JA026102](https://doi.org/10.1029/2018JA026102)
- Papaphilippou, Y., & Laskar, J. 1996, *A&A*, 307, 427
- . 1998, *A&A*, 329, 451
- Patsis, P. A. 2006, *MNRAS*, 369, L56, doi: [10.1111/j.1745-3933.2006.00174.x](https://doi.org/10.1111/j.1745-3933.2006.00174.x)
- Pfenniger, D. 1986, *A&A*, 165, 74
- Pichardo, B., Martos, M., Moreno, E., & Espresate, J. 2003, *ApJ*, 582, 230, doi: [10.1086/344592](https://doi.org/10.1086/344592)
- Poincaré, H. 1891, *Bulletin Astronomique, Serie I*, 8, 12
- Price-Whelan, A. M., Johnston, K. V., Valluri, M., et al. 2016, *MNRAS*, 455, 1079, doi: [10.1093/mnras/stv2383](https://doi.org/10.1093/mnras/stv2383)
- Ribeiro, H. V., Jauregui, M., Zunino, L., & Lenzi, E. K. 2017, *PhRvE*, 95, 062106, <https://link.aps.org/doi/10.1103/PhysRevE.95.062106>
- Rojas-Niño, A., Valenzuela, O., Pichardo, B., & Aguilar, L. A. 2012, *ApJL*, 757, L28, doi: [10.1088/2041-8205/757/2/L28](https://doi.org/10.1088/2041-8205/757/2/L28)
- Rosso, O. A., Larrondo, H. A., Martin, M. T., Plastino, A., & Fuentes, M. A. 2007, *PhRvL*, 99, 154102, doi: [10.1103/PhysRevLett.99.154102](https://doi.org/10.1103/PhysRevLett.99.154102)
- Saha, P., & Tremaine, S. 1993, *Icarus*, 106, 549, doi: [10.1006/icar.1993.1192](https://doi.org/10.1006/icar.1993.1192)
- Schaap, W. E., & van de Weygaert, R. 2000, *A&A*, 363, L29, <https://arxiv.org/abs/astro-ph/0011007>
- Schuster, H. G. 1988, *Deterministic chaos: An introduction* (2nd revised edition) (Weinheim)
- Sellwood, J. A. 2014, *Reviews of Modern Physics*, 86, 1, doi: [10.1103/RevModPhys.86.1](https://doi.org/10.1103/RevModPhys.86.1)
- Sellwood, J. A., & Debattista, V. P. 2009, *MNRAS*, 398, 1279, doi: [10.1111/j.1365-2966.2009.15219.x](https://doi.org/10.1111/j.1365-2966.2009.15219.x)
- Serinaldi, F., Zunino, L., & Rosso, O. A. 2014, *Stochastic Environmental Research and Risk Assessment*, 28, 1685, doi: [10.1007/s00477-013-0825-8](https://doi.org/10.1007/s00477-013-0825-8)
- Shannon, C. E. 1948, *The Bell System Technical Journal*, 27, 379
- Suyal, V., Prasad, A., & Singh, H. P. 2012, *Solar Physics*, 276, 407, doi: [10.1007/s11207-011-9889-0](https://doi.org/10.1007/s11207-011-9889-0)
- Suzuki, S., & Maeda, K.-I. 2000, *PhRvD*, 61, 024005, doi: [10.1103/PhysRevD.61.024005](https://doi.org/10.1103/PhysRevD.61.024005)
- Thaxton, C. S., Anderson, W. P., Gu, C., Stosic, B., & Stosic, T. 2018, *Stochastic Environmental Research and Risk Assessment*, 32, 843, doi: [10.1007/s00477-017-1434-8](https://doi.org/10.1007/s00477-017-1434-8)
- Valluri, M., Debattista, V. P., Quinn, T. R., Roškar, R., & Wadsley, J. 2012, *MNRAS*, 419, 1951, doi: [10.1111/j.1365-2966.2011.19853.x](https://doi.org/10.1111/j.1365-2966.2011.19853.x)
- Valluri, M., & Merritt, D. 1998, *ApJ*, 506, 686, doi: [10.1086/306269](https://doi.org/10.1086/306269)
- Valluri, M., Shen, J., Abbott, C., & Debattista, V. P. 2016, *ApJ*, 818, 141, doi: [10.3847/0004-637X/818/2/141](https://doi.org/10.3847/0004-637X/818/2/141)
- Varadi, F., Runnegar, B., & Ghil, M. 2003, *ApJ*, 592, 620, doi: [10.1086/375560](https://doi.org/10.1086/375560)

- Weck, P. J., Schaffner, D. A., Brown, M. R., & Wicks, R. T. 2015, *Phys. Rev. E*, 91, 023101.
<https://link.aps.org/doi/10.1103/PhysRevE.91.023101>
- Weinberg, M. D. 2015a, arXiv e-prints, arXiv:1508.06855.
<https://arxiv.org/abs/1508.06855>
- . 2015b, arXiv e-prints, arXiv:1508.05959.
<https://arxiv.org/abs/1508.05959>
- Weygand, J. M., & Kivelson, M. G. 2019, *ApJ*, 872, 59,
doi: 10.3847/1538-4357/aafda4
- Zhu, Z., White, A. E., Carter, T. A., Baek, S. G., & Terry, J. L. 2017, *Physics of Plasmas*, 24, 042301,
doi: 10.1063/1.4978784
- Zunino, L., Soriano, M. C., & Rosso, O. A. 2012, *Physical Review E*, 86, 046210
- Zunino, L., Zanin, M., Tabak, B. M., Perez, D. G., & Rosso, O. A. 2010, *Physica A: Statistical Mechanics and its Applications*, 389, 1891. <http://www.sciencedirect.com/science/article/pii/S0378437110000397>